Negative propagation effect in nonparaxial Airy beams

Pablo Vaveliuk[1,*] **and Oscar Martinez-Matos**[2]

[1]*Faculdade de Tecnologia, Servicio Nacional de Aprendizagem Industrial SENAI-Cimatec, Av. Orlando Gomes 1845 41650-010, Salvador, Bahia, Brazil*

[2]*Departamento de Óptica, Facultad de Ciencias Físicas, Universidad Complutense de Madrid, Av. Complutense s/n 28040 Madrid, Spain*

[*]*pablov@fisica.ufpb.br*

Abstract: Negative propagation is an unusual effect concerning the local sign change in the Poynting vector components of an optical beam under free propagation. We report this effect for finite-energy Airy beams in a subwavelength nonparaxial regime. This effect is due to a coupling process between propagating and evanescent plane waves forming the beam in the spectral domain and it is demonstrated for a single TE or TM mode. This is contrary to what happens for vector Bessel beams and vector X-waves, for which a complex superposition of TE and TM modes is mandatory. We also show that evanescent waves cannot contribute to the energy flux density by themselves such that a pure evanescent Airy beam is not physically realizable. The break of the shape-preserving and diffraction-free properties of Airy beams in a nonparaxial regime is exclusively caused by the propagating waves. The negative propagation effect in subwavelength nonparaxial Airy beams opens new capabilities in optical traps and tweezers, optical detection of invisibility cloacks and selective on-chip manipulation of nanoparticles.

OCIS codes: (260.2110) Electromagnetic optics; (350.5500) Propagation; (070.2580) Paraxial wave optics.

References and links

1. M. V. Berry and N. L. Balazs, "Nonspreading wave packets," Am. J. Phys. **47**, 264 –267 (1979).
2. G. A. Siviloglou and D. N. Christodoulides, "Accelerating finite energy Airy beams," Opt. Lett. **32**, 979–981 (2007).
3. G. A. Siviloglou, J. Broky, A. Dogariu, and D. N. Christodoulides,"Observation of accelerating Airy beams," Phys. Rev. Lett. **99**, 213901 (2007).
4. G. A. Siviloglou, J. Broky, A. Dogariu, and D. N. Christodoulides,"Ballistic dynamics of Airy beams," Opt. Lett. **33**, 207–209 (2008).
5. D. M. Cottrell, J. A. Davis, and T. M. Hazard, "Direct generation of accelerating Airy beams using a 3/2 phase-only pattern," Opt. Lett. **34**, 2634–2636 (2009).
6. J. A. Davis, M. J. Mitry, M. A. Bandres, I. Ruiz, K. P. McAuley, and D. M. Cottrell, "Generation of accelerating Airy and accelerating parabolic beams using phase-only patterns," Appl. Opt. **48**, 3170–3176 (2009).
7. M. A. Bandres and J. C. Gutierrez-Vega, "Airy-Gauss beams and their transformation by paraxial optical systems," Opt. Express **15**, 16719–16728 (2007).
8. J. A. Davis, M. J. Mintry, M. A. Bandres, and D. M. Cottrell, "Observation of accelerating parabolic beams," Opt. Express **16**, 12866–12871 (2008).
9. J. E. Morris, M. Mazilu, J. Baumgartl, T. Cižmár, and K. Dholakia, "Propagation characteristics of Airy beams: dependence upon spatial coherence and wavelength," Opt. Express **17**, 13236–13245 (2009).
10. M. I. Carvalho and M. Facão, "Propagation of Airy-related beams," Opt. Express **18**, 21938–21949 (2010).

#174079 - $15.00 USD Received 9 Aug 2012; revised 17 Oct 2012; accepted 19 Oct 2012; published 14 Nov 2012

11. P. Vaveliuk, G. F. Zebende, M. A. Moret and B. Ruiz, "Propagating free-space nonparaxial beams," J. Opt. Soc. Am. A **24**, 3297–3302 (2007).
12. A. V. Novitsky and D. V. Novitsky, "Nonparaxial Airy beams: role of evanescent waves," Opt. Lett. **34**, 3430–3432 (2009).
13. I. Kaminer, R. Bekenstein, J. Nemirovsky, and M. Segev, "Nondiffracting accelerating wave packets of Maxwell's equations," Phys. Rev. Lett. **108**, 163901 (2012).
14. Z. Chen, " Viewpoint: light bends itself into an arc," Phys. **5**, 44 (2012).
15. A. V. Novitsky and D. V. Novitsky, "Negative propagation of vector Bessel beams," J. Opt. Soc. Am. A **24**, 2844–2849 (2007).
16. M. A. Salem and H. Bağci, "Energy flow characteristics of vector X-waves," Opt. Express **19**, 8526–8532 (2011).
17. A. Salandrino and D. N. Christodoulides, "Airy plasmon: a nondiffracting surface wave," Opt. Lett. **35**, 2082–2084 (2010).
18. A. Minovich, A. E. Klein, N. Janunts, T. Pertsch, D. N. Neshev, and Yu. S. Kivshar, "Generation and near-field imaging of Airy surface plasmons," Phys. Rev. Lett. **107**, 116802 (2011).
19. L. Li, T. Li, S. M. Wang, C. Zhang, and S. N. Zhu, "Plasmonic Airy beam generated by in-plane diffraction," Phys. Rev. Lett. **107**, 126804 (2011).
20. P. Zhang, S. Wang, Y. Liu, X. Yin, C. Lu, Z. Chen, and X. Zhang, "Plasmonic Airy beams with dynamically controlled trajectories," Opt. Lett. **36**, 3191–3193 (2011).
21. A. Salandrino and D. N. Christodoulides, "Viewpoint: Airy plasmons defeat diffraction on the surface," Phys. **4**, 69 (2011).
22. T. Schneider, A. A. Serga, A. V. Chumak, C. W. Sandweg, S. Trudel, S. Wolff, M. P. Kostylev, V. S. Tiberkevich, A. N. Slavin, and B. Hillebrands, "Nondiffractive subwavelength wave beams in a medium with externally controlled anisotropy," Phys. Rev. Lett. **104**, 197203 (2010).
23. W. Liu, D. N. Neshev, I. V. Shadrivov, A. E. Miroshnichenko, and Yu. S. Kivshar, "Plasmonic Airy beam manipulation in linear optical potentials," Opt. Lett. **36**, 1164-1166 (2011).
24. J. W. Goodman, *Introduction to Fourier Optics*, (McGraw-Hill, New York, 1968).
25. I. M. Besieris and A. M. Shaarawi, "A note on an accelerating finite energy Airy beam," Opt. Lett. **32**, 2447–2449 (2007).
26. A. Lencina and P. Vaveliuk, "Squared-field amplitude modulus and radiation intensity nonequivalence within nonlinear slabs," Phys. Rev. E **71**, 056614 (2005).
27. P. Vaveliuk, B. Ruiz and A. Lencina, "Limits of the paraxial aproximation in laser beams," Opt. Lett. **32**, 927–929 (2007).
28. P. Vaveliuk and O. Martinez-Matos, "Physical interpretation of the paraxial estimator," Opt. Commun. **285**, 4816–4820 (2012).
29. P. Vaveliuk, "Quantifying the paraxiality for laser beams from the M^2-factor," Opt. Lett. **34**, 340–342 (2009).
30. P. Vaveliuk and O. Martinez-Matos, "Effect of ABCD transformations on beam paraxiality," Opt. Express **19**, 25944–25953 (2011).
31. Z. Zheng, B.-F. Zhang, H. Chen, J. Ding, and H.-T. Wang, "Optical trapping with focused Airy beams," Appl. Opt. **50**, 43–49 (2011).
32. M. Righini, A. S. Zelenina, C. Girard, and R. Quidant, "Parallel and selective trapping in a patterned plasmonic landscape," Nature Phys. **3**, 477–480 (2007).
33. B. Zhang and B.-I. Wu, "Electromagnetic detection of a perfect invisibility cloak," Phys. Rev. Lett. **103**, 243901 (2009).

1. Introduction

A non-square-integrable wave-packet in terms of Airy functions was firstly reported in quantum mechanics [1]. Such a wavelike solution possesses peculiar features: lack of parity symmetry about the origin and an ideal diffraction-free propagation associated with self-bending dynamics. In optics, a solution of the paraxial wave equation (PEq) was derived giving rise to the so-called finite-energy Airy beam (AiB) [2]. This beam maintains the quoted properties of the quantum wave packet but with the propagation being quasi-nondiffracting due to an exponential apodization in the field profile transforming it in a square-integrable beam. The AiB was experimentally realized by diverse phase mask encoded methods [3–6] and numerous *Airylike* beams, variants of that original finite-energy Airy beam, were widely analyzed from theoretical and experimental viewpoint [6–10]. In any case, the AiB and its generalizations have physical meaning only within a paraxial framework since the PEq is a first-order approximation of the full Helmholtz equation (HEq) [11]. Under nonparaxial conditions, the features of these parax-

#174079 - $15.00 USD Received 9 Aug 2012; revised 17 Oct 2012; accepted 19 Oct 2012; published 14 Nov 2012

ial beams should suffer strong disturbances. Nowadays, these disturbances are viewed as undesirable effects since they inhibit the self-bending and diffracting-free properties that are present in the paraxial regime. Reference [12] confirmed the breaking of those properties. The evanescent waves seem to play a key role in this, to the extent that the so-called *evanescent Airy beam*, consisting exclusively of its own evanescent waves, was proposed as a fundamental result under strong nonparaxial conditions [12]. These detrimental effects in nonparaxial AiBs encouraged the research on Airylike beams that maintain the self-bending and shape-preserving properties in that regime. Hence, the great importance of the recent derivation of nonparaxial self-bending Bessel-like beams [13] that not only conserves but also enhances those features [13, 14]. From this, one can see that the nonparaxial region is a rich source of emergence of novel unconventional features for this class of beams.

In this work, the negative propagation effect is reported under a strong nonparaxial regime for finite-energy AiBs. This is an unusual effect concerning the local sign change in the time-averaged Poynting vector components along the propagation direction of an optical beam in free space. The negative propagation was recently demonstrated for other kinds of nondiffracting structures such as vector Bessel beams [15] and vector X-waves [16]. The origin of this peculiar phenomenon for Bessel beams and X-waves is a collinear weighted superposition of TE and TM-polarization components in the real space. But the cause is quite different for AiBs. The negative propagation does occur in a single TE or TM mode and is due to a coupling process (interference-like process) between propagating and evanescent plane wave components in the spectral domain under strong nonparaxial conditions. Furthermore, this work shows that evanescent waves by themselves have null contribution to the energy flux density even under the most extreme nonparaxial conditions. Thereby, the *evanescent Airy beam* [12] is not physically realizable. At this instance, a required question naturally arises: Is it feasible to generate highly nonparaxial beams? Recent significant advances have been made in one such direction. The dielectric-metal surfaces have been demonstrated to be promising systems since Ref. [17] suggested a new class of diffraction-free surface plasmonic waves: the Airy plasmon. From that work, Airy plasmons possessing a subwavelength size of the central lobe have been generated by several groups [18–20]. The experiments performed in [18] on Airy Plasmons were in agreement with the nonparaxial theory confirming that these beams lie out of the paraxial region. The quick development in subwavelength nonparaxial AiBs open real opportunities for detection of the negative propagation effect in these dielectric-metal surfaces [21] and other class of materials [22], in particular, for the near- and mid-infrared range ($1-100\mu$m) [23].

The paper is structured as follows: Section 2 develops the theoretical framework based on the angular spectrum theory and sets the paraxial-nonparaxial limits in terms of the main beam parameters. Section 3 tackles the propagation dynamics of Airy beam under a nonparaxial regime, highlighting the conditions under which the negative propagation effect takes place. Finally, Section 4 gives the final considerations.

2. Theoretical background and paraxial-nonparaxial limit for finite-energy Airy beams

We start from a monochromatic TE-polarized solution of Maxwell's equations $\vec{E} = E_0 U(x,z) e^{i\omega t}\hat{y}$ where ω is the frequency, E_0 is a constant with electric field dimensions and U is the dimensionless field obeying the HEq in a medium of permittivity ε:

$$\left[\partial^2/\partial x^2 + \partial^2/\partial z^2 + \varepsilon\,(2\pi/\lambda)^2\right] U(x,z) = 0, \tag{1}$$

with λ being the wavelength. We introduce the spacial dimensionless variables $\tilde{x} = \varepsilon^{1/2} x/\lambda$ and $\tilde{z} = \varepsilon^{1/2} x/\lambda$. This normalization simplifies the mathematics and allows for easier interpretation of the results. The field U can be analyzed by employing the angular spectrum formalism [24].

#174079 - $15.00 USD Received 9 Aug 2012; revised 17 Oct 2012; accepted 19 Oct 2012; published 14 Nov 2012

Within it, the various spatial Fourier components can be identified as plane waves traveling in different directions. The field amplitude at any point can be calculated by adding the plane waves contributions from a given point at the initial propagation plane, taking into account the respective phase shifts. Hence,

$$U(\tilde{x},\tilde{z}) = \int_{-\infty}^{+\infty} \mathscr{U}(\tilde{p};0) e^{i2\pi\tilde{z}\sqrt{1-\tilde{p}^2}} e^{i2\pi\tilde{p}\tilde{x}} d\tilde{p}, \tag{2}$$

where $\mathscr{U}(\tilde{p};0) = \int_{-\infty}^{+\infty} d\tilde{x} U(\tilde{x},0) e^{-2\pi i\tilde{p}\tilde{x}}$ is the angular spectrum at the initial propagation plane ($\tilde{z}=0$) and the dimensionless spatial frequency $\tilde{p} = \lambda p/\varepsilon^{1/2}$ is the conjugate variable of $\tilde{x}$. For AiBs, $\mathscr{U}(\tilde{p};0)$ is Gaussian and involves a cubic phase [2–4, 25]:

$$\mathscr{U}(\tilde{p};0) = \tilde{x}_0 e^{(a-i2\pi\tilde{p}\tilde{x}_0)^3}. \tag{3}$$

The AiB is characterized by two parameters. The transverse size, x_0 (we use the dimensionless size $\tilde{x}_0 = \varepsilon^{1/2} x_0/\lambda$) that accounts for the size of the beam central lobe and the exponential truncation factor, a. This guarantees the square integrability of the beam and controls the spreading properties [2, 25]. Notice that U can be physically interpreted as having contributions of both propagating plane waves U_{pr} and evanescent plane waves U_{ev} separated by the critical spatial frequency $|\tilde{p}_c| = 1$:

$$U = U_{pr} + U_{ev}, \tag{4a}$$

$$U_{pr}(\tilde{x},\tilde{z}) = \int_{-1}^{1} \mathscr{U}(\tilde{p};0) e^{i2\pi\tilde{z}\sqrt{1-\tilde{p}^2}} e^{i2\pi\tilde{p}\tilde{x}} d\tilde{p}, \tag{4b}$$

$$U_{ev}(\tilde{x},\tilde{z}) = \int_{-\infty}^{-1} \mathscr{U}(\tilde{p};0) e^{-2\pi\tilde{z}\sqrt{\tilde{p}^2-1}} e^{i2\pi\tilde{p}\tilde{x}} d\tilde{p} + \int_{1}^{\infty} \mathscr{U}(\tilde{p};0) e^{-2\pi\tilde{z}\sqrt{\tilde{p}^2-1}} e^{i2\pi\tilde{p}\tilde{x}} d\tilde{p}. \tag{4c}$$

The angular spectrum approach was also employed in Ref. [12] but without the explicit decomposition given by Eqs. (4). As a next step, we must evaluate the spatial distribution of the radiation intensity, which is the z-component of the time-averaged Poynting vector. This can be expressed, except for a dimensional constant, as [26, 27]

$$\mathrm{S}(\tilde{x},\tilde{z}) = \mathrm{Im}\{U^* \partial U/\partial\tilde{z}\}. \tag{5a}$$

By replacing (4a) into (5a), one obtains

$$\mathrm{S} = \mathrm{S}_{pr} + \mathrm{S}_{ev} + \mathrm{S}_{cr}, \tag{5b}$$

where

$$\mathrm{S}_j = \mathrm{Im}\left\{U_j^* \frac{\partial U_j}{\partial\tilde{z}}\right\};\ \mathrm{S}_{cr} = \mathrm{Im}\left\{U_{pr}^* \frac{\partial U_{ev}}{\partial\tilde{z}} + U_{ev}^* \frac{\partial U_{pr}}{\partial\tilde{z}}\right\}, \tag{5c}$$

with $j = pr, ev$. The energy flow density is then constituted by three terms: the propagating and evanescent plane waves and a *interference-like* term, product of the coupled contribution of both components. Now, we have the full machinery to analyze the propagation dynamics of nonparaxial Airy beams. But before we do that, it is necessary to accurately delimit the paraxial-nonparaxial range in terms of the AiB parameters. Such a range can be quantified by a useful parameter, the *paraxial estimator* ($\mathscr{P}$) introduced in Ref. [27]. Its definition is based on the comparison between the propagation invariants associated to HEq and PEq. From that, the range of $\mathscr{P}$ lies between the interval $(-\infty, 1)$, and the limit $\mathscr{P} \to 1$ guarantees the paraxial

#174079 - $15.00 USD Received 9 Aug 2012; revised 17 Oct 2012; accepted 19 Oct 2012; published 14 Nov 2012

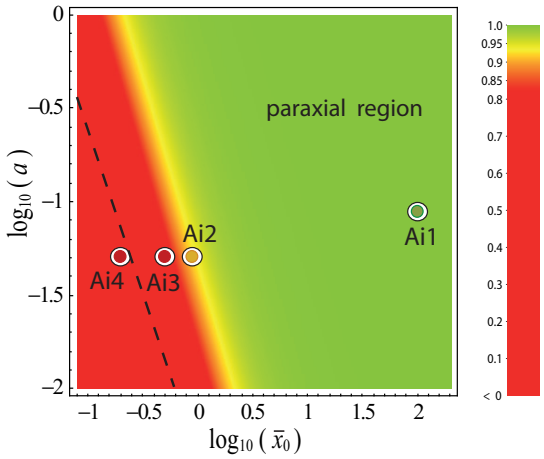

Fig. 1. Map of $\mathscr{P}$ vs. ($\tilde{x}_0$, a). The points set the different configurations of Airy beams in this paraxial-nonparaxial map with the following values of the paraxial estimator. For Ai1: $\mathscr{P} = 0.999996$; For Ai2: $\mathscr{P} = 0.92$; For Ai3: $\mathscr{P} = 0.75$; For Ai4: $\mathscr{P} = -0.58$. The dashing line corresponds to $\mathscr{P} = 0$.

approximation validity [27]. As $\mathscr{P}$ departures from unit, the beam becomes more and more nonparaxial [27, 28]. $\mathscr{P}$ can be calculated from the angular spectrum of the beam [29]. We omit the explicit calculi here but a simple analytical expression for $\mathscr{P}$ can be easily obtained from the AiB angular spectrum for $\tilde{z} \geq 0$:

$$\mathscr{P} = 1 - 1/(32\pi^2 a\tilde{x}_0^2). \tag{6}$$

The criterion to set the *paraxiality scale* of $\mathscr{P}$ follows the used for the fundamental Gaussian mode as emphasized in [30]. As such, the paraxial approximation begins to be a questionable hypotheses for $\mathscr{P}$-values lower than 0.94. Figure 1 depicts a density plot of $\mathscr{P}$ in terms of $\tilde{x}_0$ and a. The interval of both parameters covers a wide range of feasible experimental values. The points in Fig. 1 indicate certain configurations of interest that will be analyzed here. The configuration Ai1 represents a typical setup for Aibs generated in free space by mask encoded methods: $\tilde{x}_0 \approx 100$ and $a_x \approx 0.08$ [3, 4]. Notice that the paraxial regime is fully guaranteed for this set of parameters. There is a practically null chance to get out of the paraxial region by these beam generation methods. By using Eqs. (5), our simulations showed a full agreement with the results given by the celebrated paraxial solution [2–4]. But, what will happen for different nonparaxial setups? We will address that in the next section.

3. Nonparaxial Airy beams and negative propagation effect

The paraxial-nonparaxial map, illustrated in Fig. 1, points out the range of values of the beam parameters for which the paraxial-nonparaxial transition takes place. It is clear that the nonparaxial regime implies subwavelength values of $\tilde{x}_0$ for the typical values of a (≤ 0.08). Let us study several representative nonparaxial configurations that are indicated in Fig. 1.The configuration Ai2 ($\tilde{x}_0 = 0.9$ and $a_x = 0.05$) could be classified as a slight-moderate nonparaxial configuration according to its value of $\mathscr{P}$. It was experimentally obtained in plasmonics [18] where measures of the deflection of the main lobe were well-adjusted from the nonparaxial theory. The principal features of this configuration are summarized in Figs. 2(a)-(b). The nonparaxial AiB behaves as a paraxial one possessing accelerating properties up to a given distance

#174079 - $15.00 USD Received 9 Aug 2012; revised 17 Oct 2012; accepted 19 Oct 2012; published 14 Nov 2012

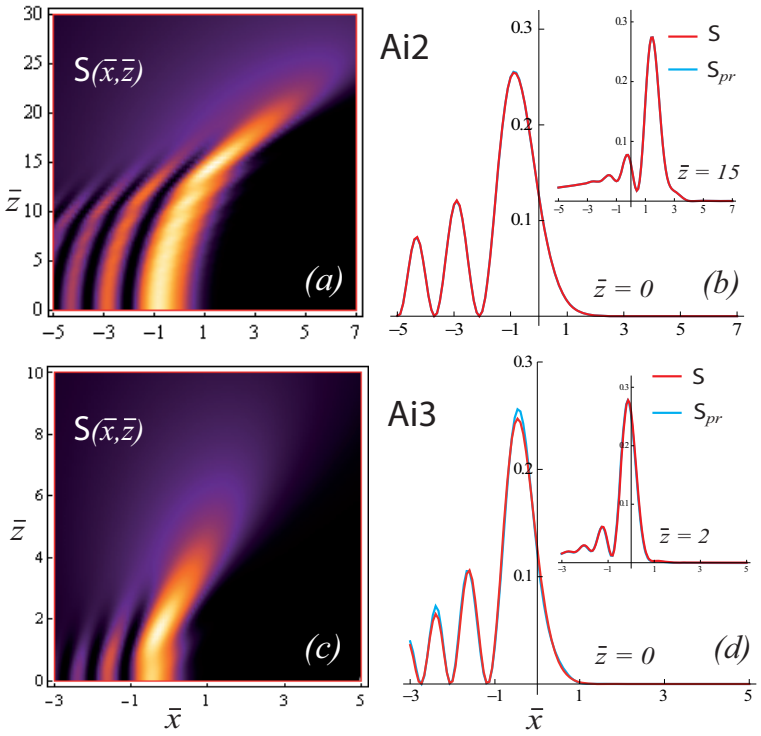

Fig. 2. Features of a nonparaxial Airy beam for (a)-(b) configuration Ai2 and (c)-(d) configuration Ai3. (a) and (c) Energy flow density as a function of normalized spatial coordinates. (b) and (d) Profiles of both the total energy flow density and the energy flow density due to the propagating plane waves. Clearly, the contribution of evanescent waves is null for both configurations in the overall spatial range.

before break up. The *paraxial-nonparaxial breaking region* happens in this case around $\tilde{z} \approx 15$ as Fig. 2(a) shows. The nonparaxial disturbance produces a quick disappearance of the secondary lobes and a greater lateral shift of the principal lobe over a little distance just before a strong beam self-divergence. This nonparaxial effect is exclusively due to the propagating waves since the profiles corresponding to $\mathtt{S}$ and $\mathtt{S}_{pr}$ fully overlap along the overall propagation coordinate as Fig. 2(b) illustrates. There is no influence from the evanescent waves. What happens in a evermore nonparaxial regime? According as $\tilde{x}_0 \to 0$, the disturbance takes place at lower values of $\tilde{z}$. The configuration Ai3 is characterized by a important subwavelength size $\tilde{x}_0 = 0.5$ and could be catalogued as a moderate-strong nonparaxial configuration according its $\mathscr{P}$-value. The results on the propagation dynamics are depicted in Figs. 2(c)-(d). The *paraxial-nonparaxial breaking region* is now located at $\tilde{z} \approx 2$ as Fig. 2(c) shows. Ai3 behaves similarly to Ai2 with no further nonparaxial effects and a still negligible evanescent wave influence. In fact, $\mathtt{S}$ and $\mathtt{S}_{pr}$ overlap along the overall propagation coordinate as Fig. 2(d) confirms. This rules out the current belief that the self-bending breaking and the strong spreading of these beams are caused by the evanescent waves. Is it then feasible to have a nonparaxial effect tied to the evanescent waves? To elucidate this question we analytically analyze the evanescent energy flow density, $\mathtt{S}_{ev}$, in Eq. (5c). By expanding $\mathscr{U}(\tilde{p};0)$ [given by Eq. (3)] and $\exp(i2\pi\tilde{p}\tilde{x})$ in terms of their respective real and imaginary parts and by using the symmetry properties of sine and cosine functions, it is straightforward to prove that the imaginary part of $U^{*}_{ev}\partial U_{ev}/\partial\tilde{z}$

#174079 - $15.00 USD Received 9 Aug 2012; revised 17 Oct 2012; accepted 19 Oct 2012; published 14 Nov 2012

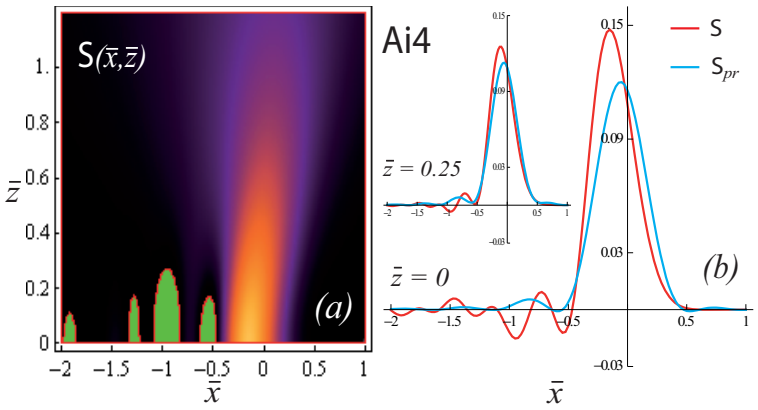

Fig. 3. z-component of the time-averaged Poynting vector for a Airy beam in the configuration Ai4. (a) Such a magnitude as a function of normalized spatial coordinates. S is negative at the green regions. (b) Profiles of both the total energy flow density and the energy flow density due to the propagating plane waves at $\tilde{z}=0$ and $\tilde{z}=0.25$ (inset). Clearly, both magnitudes differs due to a non-null coupling term between propagating and evanescent waves. This last term is the responsible by the negative propagation. Out of the region of influence of evanescent waves, S and S_{pr} are equivalent.

is null such that

$$\mathrm{S}_{ev}(\tilde{x},\tilde{z})=0 \tag{7}$$

is always fulfilled. This result was fully verified by our numerical simulations. Therefore, in no case there is a contribution of pure evanescent waves to the total energy flow density, even in the most extreme nonparaxial regime. Necessarily, these waves can only manifest through the coupling term between evanescent and propagating waves. This key result defeats any real possibility of existence of the *evanescent Airy beam* as proposed in [12]. Now, we investigate if the coupling term has some effective contribution to the energy flux density by reducing the beam size. A recent work [28] emphasized that negative values of $\mathscr{P}$ are related to some effective role of the evanescent waves on the nonparaxial dynamics. Hence, it would be a good idea to analyze a nonparaxial configuration with $\mathscr{P}<0$ to see if there exists some contribution of S_{cr} to the radiation intensity. One must have care in choosing a potentially achievable nonparaxial configuration to avoid an elegant theoretical result but that lacks physical insight. Notice that the configuration Ai4 in Fig. 1 possesses a slightly negative $\mathscr{P}$-value and is characterized by $\tilde{x}_0=0.2$. Such a configuration has not been experimentally obtained to the best of our knowledge. However, the quick development in the generation of unconventional beams open further opportunities for highly nonparaxial Airy beams in dielectric-metal surfaces [21] and other class of materials [22]. Such a configuration would be possible for higher spectral ranges as the near- and mid-infrared regions ($1-100\mu$m), where AiBs began to be synthesized [23].

The numerical results for the configuration Ai4 are illustrated in Fig. 3. Part (a) of this figure shows that the self-bending and shape-preserving properties are completely lost. The beam propagates approximately a wavelength before a strong spreading. The paraxial-nonparaxial breaking region is located at the beginning of the propagation and all the beam dynamics happens in a subwavelength region. In spite of the full break on accelerating and diffraction-free properties, a peculiar new nonparaxial effect appears: The secondary peaks of the z-component of the time-averaged Poynting vector S presents negative values along the propagation coordinates. The spatial range of this phenomenon (up to $\tilde{z}\approx 0.25$) is approximately 25% of the total

#174079 - $15.00 USD Received 9 Aug 2012; revised 17 Oct 2012; accepted 19 Oct 2012; published 14 Nov 2012

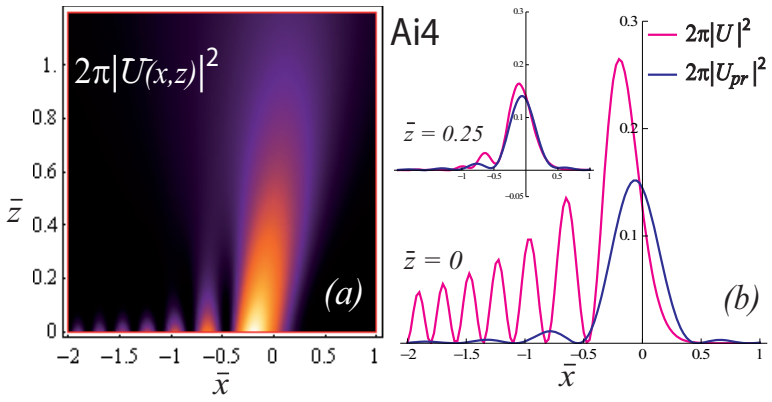

Fig. 4. Squared-field amplitude modulus of an Airy beam for the configuration Ai4. (a) Such a magnitude as a function of normalized spatial coordinates. (b) Profiles of both the total squared-field amplitude modulus and that due to the propagating plane waves at $\tilde{z} = 0$ and $\tilde{z} = 0.25$ (inset). If $2\pi|U|^2$ is taken as the energy flux density, the negative propagation effect does not take place.

propagation range of the beam as indicates the green region in Fig. 3(a). The amplitude of the major of negative peaks is greater than 10% of the principal peak. These data suggest that this effect would be highly detectable if this configuration would be carried out experimentally. Of course, this effect will be even greater if the beam size decreases further. The coupling term is fully responsible by such a phenomenon as shown by the comparison between S and S_{pr} [Fig. 3(b)]. The magnitudes are very different in the near field region where the evanescent waves exert influence. As the beam propagates away from the near field region, the dynamics is exclusively governed by the propagating waves and both profiles begin to be practically equivalents after $\tilde{z} = 0.25$. A great advantage is that this negative propagation takes place for a single TE or TM mode contrary to what happens for Bessel beams and X-waves [15, 16], which require a complex superposition of TE and TM modes, hard to be performed in a experimental way. From this finding, the subwavelength nonparaxial Airy beam may not be viewed as an undesirable one since this novel effect opens promising opportunities in certain applications. For instance, in optical tweezers it can offers a novel way of optically manipulating micro and nano-particles. In fact, the variation in sign of the Poynting vector could create multiple traps for confining particles in the vicinity of the positive-negative intensity lobes. This trapping pattern could be more stable than that created by focused Airy beams [31]. Furthermore, the transition from 3D to 2D tweezers is possible by exploiting evanescent fields bound at interfaces to achieve subwavelength trapping volumes. The nonparaxial AiBs opens a huge potential towards the elaboration of future lab-on-a-chip devices entirely operated with light [32]. On the other hand, the negative propagation effect could also be used as an effective tool in the detection of invisibility cloacks. This nonparaxial AiB could serve as an additional bridge from the flat mechanical space to the curved electromagnetic space by means of the interaction with a charged particle through a perfect invisibility cloak [33].

As a final question, one could ask why the negative propagation effect in AiBs was not previously reported. This is closely related to the nonequivalence between the squared-field amplitude modulus and radiation intensity under strong nonparaxial conditions. For instance, in nonlinear optics, one such nonequivalence led to the postulation of the so-called *Poynting medium* [26]. In the case of linear media, both magnitudes hold equivalent for non strongly nonparaxial conditions as for configurations Ai1, Ai2 and inclusive Ai3. But this is broken for

#174079 - $15.00 USD Received 9 Aug 2012; revised 17 Oct 2012; accepted 19 Oct 2012; published 14 Nov 2012

the configuration Ai4. Notice that the negative propagation effect is forbidden if the radiation intensity is taken as the squared-field amplitude modulus as Fig. 4 clearly shows. The contribution of the evanescent waves to this "pseudo-intensity" magnitude, $2\pi|U|^2$, is from two terms: one corresponding to pure evanescent waves, $2\pi|U_{ev}|^2$, and another corresponding to the coupling between both kinds of waves, $4\pi\mathrm{Re}(U_{pr}U_{ev}^*)$. The total "pseudo-intensity" then results in many intense and positive secondary peaks in the neighborhood of the starting propagation plane [see Fig. 4(a)]. It also differs strongly from the "propagating wave pseudo-intensity", $2\pi|U_{pr}|^2$, as Fig. 4(b) shows. The secondary peaks quickly decay as the beam propagates. As an example, at distance $\tilde{z} = 0.1$ only the first secondary peak survives. The *evanescent Airy beam* [12] could take place in this "pseudo-energetic representation".

4. Concluding remarks

To summarize, we have reported the negative propagation effect in subwavelength nonparaxial Airy beams that is due to the coupling between propagating and evanescent plane waves. This effect can occur for a single TE(TM)-mode contrary to what happens for Bessel beams and X-waves. We also show that the evanescent waves cannot contribute to the energy flux density by themselves such that a pure evanescent Airy beam is physically forbidden. The breaking of the shape-preserving and diffraction-free properties of Airy beams in the nonparaxial regime are caused exclusively by the propagating waves. This work could have profound implications in several applications since it brings the usefulness of (before undesired) nonparaxial Airy beams to a subwavelength regime. This opens new opportunities in optical traps and tweezers for manipulating micro- and nanoparticles, optical detection of invisibility cloacks and selective on-chip manipulation of nanoparticles.

Acknowledgments

The Authors thank Valéria Loureiro da Silva for valuable advice. Financial support from the Conselho Nacional de Desenvolvimento Cientifico e Tecnologico (CNPq), Brazil, under project 477260/2010-1 and Spanish Ministry of Science and Innovation under projects TEC 2008-04105 and TEC 2011-23629 is acknowledged. P.V. acknowledges a PQ fellowship of CNPq. The publication of this work was supported by Servicio Nacional de Aprendizagem Industrial (SENAI)-DR/Bahia, Brazil.

#174079 - $15.00 USD Received 9 Aug 2012; revised 17 Oct 2012; accepted 19 Oct 2012; published 14 Nov 2012